Special Issue on "Medicinal Chemistry"

J. Indian Chem. Soc.,
Vol. 97, August 2020, pp. 1217-1225

Anticancer activity of imidazole fused quinoxalines via human topoisomerase inhibition

Gaurav Joshi and Raj Kumar*

Department of Pharmaceutical Sciences and Natural Products, Central University of Punjab, Bathinda-151 001, Punjab, India

E-mail: raj.khunger@gmail.com, raj.khunger@cup.edu.in

Manuscript received online 15 July 2020, accepted 29 July 2020

We herein report design, synthesis of imidazo[1,2-*a*]quinoxaline (**4A-4E**) via acid-catalyzed Pictet-Spengler (PS) reaction, and their anticancer assessment through inhibition of human topoisomerases. Two compounds **4D** and **4E** were found to be dual inhibitors of human topoisomerases and possessed anticancer potential at the low micromolar concentration (IC_{50} < 4.5 μM) in A549 (lung cancer), HT-29 (colon cancer) and MDA-MB-231 (breast cancer) cells. The molecules were also able to alter the intracellular ROS levels inside cancer cells and led to apoptosis via the mitochondrial independent pathway.

Keywords: Anticancer, imidazo[1,2-*a*]quinoxalines, topoisomerases, Pictet-Spengler reaction, molecular modeling.

Introduction

Among various oncology targets, human topoisomerases (hTopos) are the second most abundant nuclear proteins[1], which are widely studied and considered as vital targets to halt the cancer prognosis[2]. hTopos are classified into Human DNA topoisomerases I and II (hTopo I and hTopo II). hTopo I is a non-ATP dependent enzyme that catalyzes the temporary breakage of DNA, one strand at a time, and the succeeding re-joining of the strands[3]. Whereas, Topo II is a dimeric and ATP-dependant enzyme belonging to the ATP kinase subfamily. The hTopo II, depending upon its molecular mechanism, is further classified into two classes, i.e. Topo IIα and Topo IIβ, both of which are isozymes[3b] and have a similar catalytic site but perform different biological functions. Topo IIα is associated with cell division, whereas Topo IIβ is involved in cell differentiation[3c]. The researchers have investigated that there is a compensatory effect between Topo I and II, indicating if one topoisomerase gets inhibited or its expression gets reduced, the other will compensate for the decrement, and its expression will rise subsequently[4]. Several drugs have now been identified that target both Topo I and Topo II simultaneously[5]. The dual hTopo I and II inhibitors reported so far are classified into three categories; the major category includes DNA intercalator class (e.g. DACA, intoplicine, A35, TAS103); the second category includes hybrid molecules designed by physically linking separate Topo I and Topo II inhibitors, although they allow the possibility of dual inhibition but failed to correspond to pharmacokinetics parameters owing to their higher molecular weights (e.g. ellipticine-distamycin hybrids). The last category includes modified candidates that possess an enhanced potential for dual inhibition. Examples include campthothecin based modified candidate (e.g. BN 80927) and etoposide based modified candidate (e.g. tafluposide)[4,6]. The relevant chemical structures of dual inhibitors are reported in Fig. 1.

The dual inhibitors, therefore, are a better option due to the following essential considerations: (i) treatment involving selective Topo II inhibitors precipitates secondary malignancies via chromosomal translocations; and (ii) development of drug-resistance during long-term clinical therapies[7]. Also, it has been hypothesized that dual inhibitors might inhibit overlapping functions in DNA metabolism, providing an enhanced anticancer activity. Further, numerous research trials provide insights that sequential administration of hTopo II inhibitor (etoposide) with hTopo I inhibitor (topotecan, irinotecan) leads to an antagonistic effect in contrast to synergism, including severe life-threatening anemia and neutropenia[8]. Therefore, it is suggested and highly recommended that a single agent possessing the property of dual inhibition of Topos affects a larger cancer cell population with enhanced anticancer potential. In the current research, we have focused on the development of dual hTopos inhibitors based on imidazo[1,2-*a*]quinoxaline scaffolds.

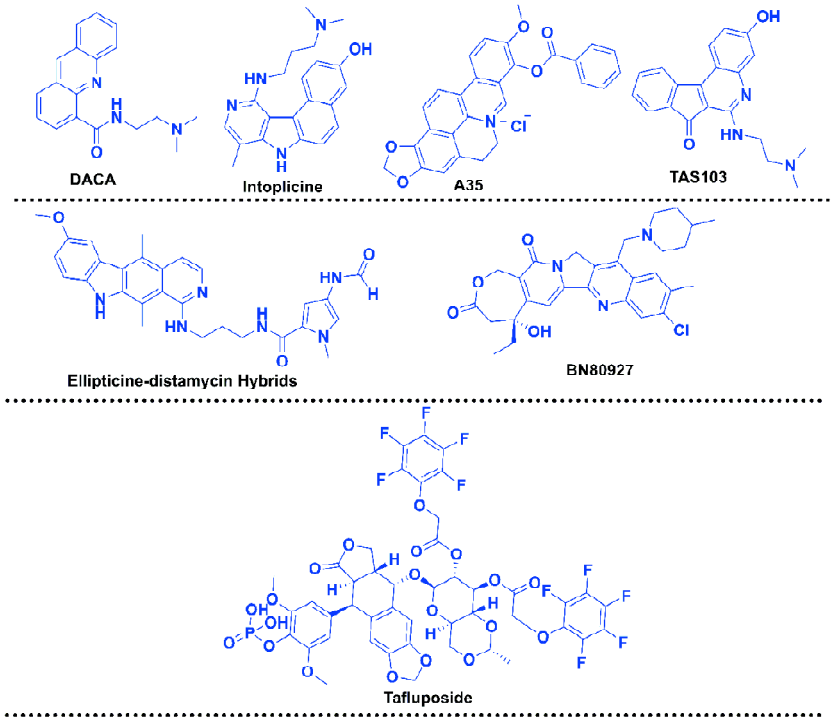

Fig. 1. Reported dual inhibitors of hTopo I and II.

Experimental

All the reagents for chemical synthesis were purchased from Sigma-Aldrich, Sisco Research Laboratory, Loba-Chemie Pvt. Ltd., India and were not further refined for purification. Monitoring of reaction progression was done using Thin Layer Chromatography (TLC) (pre-coated Merck TLC plates) using gradient concentration of petroleum ether/ethyl acetate as the mobile phase, and detection was performed in UV/fluorescent analysis cabinet. The solvent was concentrated using the ILMVAC rotary evaporator. Flash chromatography (Biotage) was used for the purification of final compounds. Stuart melting point apparatus (SMP-30) was used for recording the melting points of final synthetics. Bruker FT-IR spectrophotometer and Shimadzu GC-MS (DST-FIST sponsored and in CIL) were used for obtaining the IR and mass spectra. NMR and HRMS spectra were outsourced and recorded at IIT Ropar, Punjab.

For the biological experiments, cell culture reagents, including RPMI 1640 and DMEM media, penicillin/streptomycin antibiotic solution, phosphate buffer saline, fetal bovine serum, and biological grade DMSO were purchased from Hi-Media. Topo assay kits were purchased from TopoGen. Assays kits for (Reactive Oxygen Species) ROS, JC-1 were purchased from molecular probes and Thermo Fisher Scientific. Plastic wares were purchased from Corning and Abdos. Normal and cancer cells for experiments were procured from NCCS, Pune, India. *In vitro* assays were performed as per the protocol no. CUPB/cc/14/IEC/4483 approved by the Institutional Ethics Committee of Central University of Punjab, Bathinda.

Chemistry

*N-(2-Amino-1,2-dicyano-vinyl)-formimydic acid ethyl ester (**2**):*

To a suspension of **1** (3 g, 27.75 mmol) in 1,4-dioxane (20 ml), was added $CH(OEt)_3$ (4.5 mL). The mixture was heated at 80°C for 6 h (TLC). The reaction mixture was evaporated using a rotary evaporator, dark brown solid obtained was extracted with diethyl ether (6×20 mL) and kept overnight. The desired product **2** was obtained as yellow needles and was used for the next step without further purification. Yield: 75%; yellow solid; m.p. 134–136°C [Lit.[9] 135°C].

*N-(2-Amino-1,2-dicyano-vinyl)-N´-(2-amino-phenyl) formimidine (**3**):*

To a suspension of **2** (3 g, 18.28 mmol) in methanol (1.5 mL) was added *o*-phenylenediamine (1.85 g, 17.14 mmol) and aniline hydrochloride (2.7 mg, 0.021 mmol). The reaction mixture was stirred for 5 h at rt. The precipitate so obtained was filtered, washed with diethyl ether, and dried to afford **3**. Yield: 79%; brown solid; m.p. 118–120°C [Lit.[9,10] 119–121°C].

*5-Amino-1-(2-amino- phenyl)-1H-imidazole-4-carbonitrile (**4**):*

To a suspension of **3 (**1 g, 4.42 mmol) in water (1 mL), added 1 *M* aqueous KOH solution (15 mL) and was stirred for 6 h at rt (TLC). The mixture was extracted with EtOAc (10 mL×3). The organic layer was washed with water, brine, dried over anhydrous Na_2SO_4, and concentrated under vacuum using a rotary evaporator to afford **4**. The crude product was recrystallized from EtOAc. Yield: 89%, yellowish solid; m.p. 195–197°C [Lit.[10] 196–198°C]. HRMS (TOF-ESI) Calcd. for $C_{10}H_9N_5$, 199.2200 $[M]^+$; observed: 199.9258 $[M+H]^+$.

Representative procedure for the synthesis of target compounds:

*1-Amino-4-(3,4,5-trimethoxyphenyl)imidazo[1,2-a]quinoxaline-2-carbonitrile (**4A**):*

To a suspension mixture of **4** (100 mg, 0.502 mmol) in methanol (qs) was added 3,4,5-trimethoxybenzaldehyde (136.5 mg, 0.693 mmol) (**a**) and *p*-TsOH (1 mol %), used as catalyst. The reaction mixture was heated under reflux at 80°C for 3 h. After the completion of the reaction (TLC), methanol was evaporated from the reaction mixture, concentrated under vacuum using a rotary evaporator, extracted with ethyl acetate, dried and purified via flash chromatography (EtOAc: Pet ether: 1.5:8.5). Yield: 81%; brownish solid, m.p. 209–211°C [Lit.[10] 211–213°C]. ^{1}H NMR (400 MHz, $CDCl_3$, TMS = 0) δ: 3.94 (3H, s), 4.03 (6H, s), 4.53 (2H, s; D_2O exchangeable NH_2), 7.64–7.60 (2H, m), 7.96 (2H, s), 8.14 (1H, d, *J* 8 Hz), 8.53 (1H, m); ^{13}C NMR (100 MHz, $CDCl_3$, TMS = 0) δ: 56.39, 61.09, 104.19, 107.20, 114.82, 127.45, 127.53, 128.14, 130.40, 130.83, 133.59, 136.57, 140.67, 142.20, 149.63, 153.02. HRMS (TOF-ESI) Calcd. for $C_{20}H_{17}N_5O_3$, 375.1331 $[M]^+$; observed: 376.1349 $[M+H]^+$.

The remaining target compounds 3-amino-10-oxo-10,11,12,12*a*-tetrahydroimidazo[1,2-*a*]pyrrolo[2,1-*c*]quinoxaline-2-carbonitrile (**4B**), 1-amino-4-(chloromethyl)-4-phenyl-4,5-dihydroimidazo[1,2-*a*]quinoxaline-2-carbonitrile (**4C**), (*E*)-4-methyl-1-((3-oxo-1-phenylbutyl)amino)-4-styryl-4,5-dihydroimidazo[1,2-*a*]quinoxaline-2-carbonitrile (**4D**), and 1-amino-4-hydroxy-4-(phenylamino)-4,5-dihydroimidazo[1,2-*a*]quinoxaline-2-carbonitrile (**4E**) were synthesized as per the standardized protocol and their physical data (m.p., NMR, IR and HRMS) were in accordance with their reported values[10].

Drug design and molecular modelling:

The molecules were designed and developed on the basis of reported conserved interaction of dual inhibitor TAS-103 within active cavities of hTopo I and II in comparison to camptothecin and etoposide[11]. The representative compound of the series (**4E**) was docked into the active site of Topo I (PDB ID: 1T8I)[12] and Topo II (PDB ID: 3QX3)[13]. The docking studies were performed using AutoDock Vina. The proteins and ligands were prepared and saved using pdbqt file format. After refinement, autogrid module assisted in grid generation and finally followed by molecular docking.

Biology

Topoisomerase assay:

The assays were performed using our previous protocols as well as considering manufacturer protocol[6d,14]. For hTopo II assay, kinetoplast DNA (kDNA) was used as a substrate, and etoposide was taken as the positive control. Samples were mixed with 10X loading dye and were resolved on a 1% agarose gel electrophoresis unitin non-EB, TAE buffer. Topo I relaxation assay was performed on negatively supercoiled DNA pBR322. Investigational compounds or CPT and Topo I was incubated at 37°C for 30 min. On completion of digestion, samples were subjected to gel electrophoresis on 1% agarose gel. Visualization of both reactions was performed using Gel Doc^{TM} EZ imager (BioRad) and quantified by image Lab (BioRad).

Cell maintenance and culture:

The cell culturing was done as per our previous protocols[6d,14]. Briefly, cells were grown in culture flasks or Petri plates using DMEM media, supplemented with 10% fetal bovine serum (FBS), 1X penicillin-streptomycin antibiotic solution. The cells were maintained inside an incubator at a temperature of 37°C and a humidified atmosphere containing 5% CO_2.

Antiproliferative assay:

The antiproliferative assay was performed as per our previous protocols using MTT dye[6d,14]. In brief, approximately 10^3 cells were seeded in each well of 96 well plates. After proper synchronization (serum-starved), cells were replenished with complete media. The treatment was given when confluency reached 80% at three varying concentrations (1, 5, and 25 μM) of test and standard samples for 48 h. After specified incubation time, the media was discarded, and cells were washed using 1X PBS and were replenished with MTT dye (10 μL) prepared using 5 mg/mL solution in PBS (1X). The plate was incubated for 4 h and formazan crystals thus formed were dissolved in DMSO and absorbance was read using a microplate reader at 570 nm. IC_{50} was calculated using Origin software.

Analysis of secondary anticancer parameters:

To analyze secondary anticancer mechanisms, MDA-MB-231 cells were incubated for 48 h after treatment with test and control samples at their sub-IC_{50} concentrations. Cellular samples after treatment were harvested for staining by transferring (approximately 10^6 cells per tube). The cells were then centrifuged at 1200 rpm for 5 min and washed with 1X PBS. The suspended cells were stained and incubated for 30 min at room temperature in the dark. The fluorescence intensity was measured using the BD C6 flow cytometer using our previous protocols. Reactive Oxygen Species (ROS) assay was analyzed using H_2DCFDA (2′,7′-dichlorodihydrofluorescein diacetate) dye. The Mitochondrial Permeability, as altered by investigational samples, was analyzed using JC-1 (5,5′,6,6′-tetrachloro-1,1′,3,′-tetraethylimidacarbocyanine iodide) dye. The mode of cell death was deduced using Annexin V vs PI assay using Annexin V and propidium iodide dye[6d,14].

Results and discussion

Drug design:

The molecules were designed and developed on the basis of reported conserved interaction of dual inhibitor TAS-103 within cavities of hTopo I and II. The representative compound of the series (**4E**) was docked into the active site of Topo I (PDB ID: 1T8I)[12] and Topo II (PDB ID: 3QX3)[13]. The molecular modeling insight important interactions of TAS-103 in hTopo I that include π-π stacking of pyridine and pyrrole ring with deoxy guanine (TGP, C-11), π-cation interaction of Lys532 with the phenolic ring, and H-bond of the hydroxy group of the phenolic ring with Asp533. The **4E** also exhibited similar interactions, which include π-π stacking of imidazole and phenyl ring with TGP(C-11), and additional π-π stacking between phenyl and deoxyadenosine (DA). Further, the nitrogen of *N*-methylaniline and secondary -OH group exhibited H-bond interaction with deoxy thymine (DT) and TGP, respectively. The analysis also revealed that the compound **4E** exhibited much better binding affinity (dock score: –7.493 kcal/mol) within hTopo I as compared to TAS-103 (dock score: –6.032 kcal/mol) (see Fig. 2A). Next, the interaction of TAS-103 in hTopo II revealed H-bond interaction of lone pair of secondary -*N*H with Arg503, whereas phenolic -*O*H exhibited salt bridge interaction with the same amino acid. The interaction was found to be conserved in **4E**. The phenolic and aryl ring were involved in π-π stacking with DG, with phenyl ring showing additional π-π stacking with Arg503. The lone pair of -*N*H (ring system) made H-bond interaction with Arg503, whereas the secondary -OH group was involved in H-bonding with DT. Similarly, binding affinity exposed better attraction and active site occupation by **4E** (dock score: –9.516 kcal/mol) as compared to TAS-103 (dock score: –7.287 kcal/mol) (see Fig. 2B). Further, the binding pattern revealed that **4E** binds in a similar mode with TAS-103 within the active domain of hTopo I (Fig. 2C) and II (Fig. 2D).

Chemistry:

The target molecules (**4A**-**4E**) were synthesized based on our previously reported procedure via a modified Pictet-Spengler (PS) reaction[10]. In brief, target compounds were synthesized via a common intermediate 5-amino-1-(2-aminophenyl)-1*H*-imidazole-4-carbonitrile (**4**) obtained via condensation of diaminomaleonitrile (**1**) with $CH(OEt)_3$ in 1,4-dioxane to afford forimidate ester **2**[9a] which, in turn, underwent substitution reaction with *o*-phenylenediamine under the catalytic influence of $PhNH_2$.HCl to form **3** (Scheme 1). The reaction proceeds via nucleophilic attack of one of the nitrogen's lone pair of *o*-phenylenediamine on the electrophilic carbon atom of **2** followed by loss of one molecule of EtOH. The intermediate **3** subsequently undergoes ring formation under basic conditions (aq. KOH solution) to afford **4**, which was further reacted with a variety of electrophiles under reflux condition using *p*-TsOH (1 mol%) as a catalyst to afford the target compounds. The reaction of 3,4,5-trimethoxy

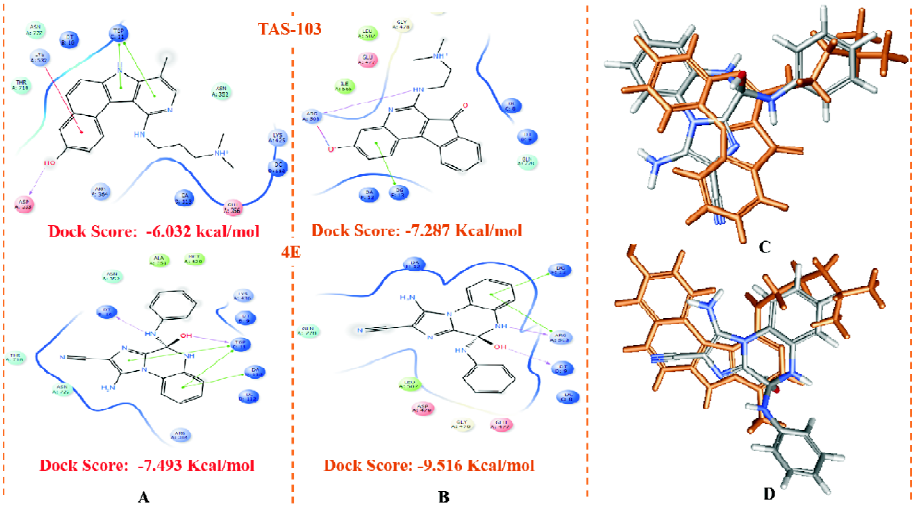

Fig. 2. (A) Interaction of **4E** and **TAS-103** within active site of hTopo I (PDB ID: 1T8I); (B) Interaction of **4E** and **TAS-103** within active site of hTopo II (PDB ID: 3QX3); (C) Overlapping interaction diagram of **4E** and **TAS-103** within the active sites of hTopo I and Topo II; (D) For representation purpose **4E** is embodied with grey color and **TAS-103** is denoted with brown.

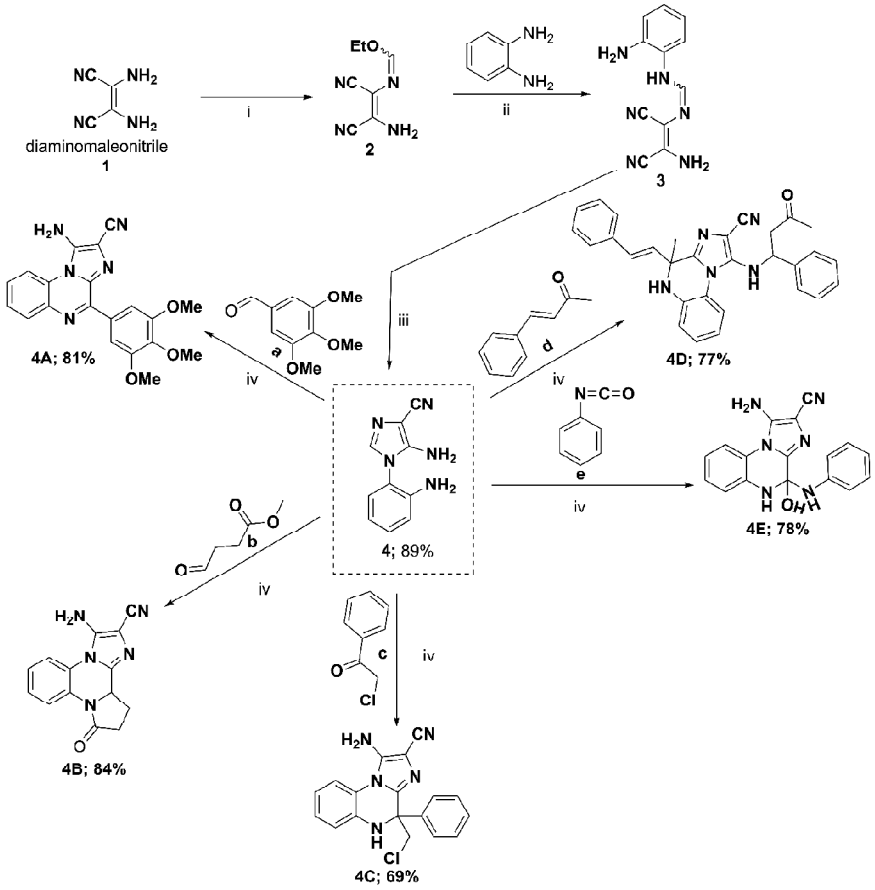

Scheme 1. Synthesis of substrate 4, and products **(4A-4E)**. Reaction conditions: (i) $CH(OEt)_3$, 1,4-dioxane, reflux, 6 h; (ii) $PhNH_2$.HCl (*cat.*), EtOH, rt, 5 h; (iii) KOH (1 *M*), H_2O, rt, 6 h; (iv) *p*-TSA, MeOH reflux, 80°C, 3–4 h.

benzaldehyde **(a)** with **4** resulted in the formation of modified PS product **4A**. Interestingly, reaction of methyl 4-oxobutanoate **(b)** with **4** led to the synthesis of **4B**, which in addition to modified PS reaction, underwent nucleophilic attack by nitrogen atom on carbonyl ester thus forming a five-membered ring. In another reaction of **4** with phenacyl chloride **(c)**, the formation of PS product **(4c)** took place via an imine pathway. Further reaction of **4** with benzalacetone **(d)** led to the formation of **4D** via PS reaction at *C*-2 of imidazole and also underwent aza-Michael addition at β-carbon of **d**. Lastly, the reaction of **4** with phenyl isocyanate **(e)** led to the formation of another modified PS product **4E** with a free secondary alcohol functionality.

Biology:

Initially, the molecules **4A-4E** were assessed for their hTopos inhibitory potential. hTopo II based decatenation assay revealed (Fig. 3) that compounds **4D** and **4E** were potent hTopo II inhibitors as compared to etoposide. However, the compounds **4A**-**4C** also inhibited the decatenation of kDNA. Further, the compounds **4B**-**4E** profoundly inhibited the relaxation process of supercoiled DNA, leading to inhibition of hTopo I (Fig. 4). The results indicated compounds **4D** and **4E** have the potential to act as dual inhibitors of hTopo I and II.

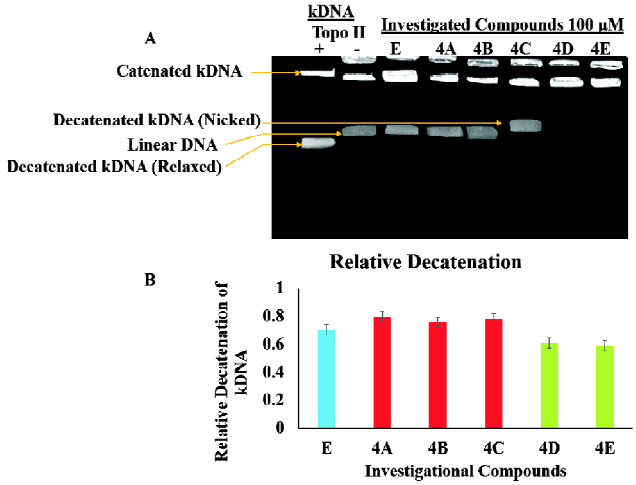

Fig. 3. (A) Agarose gel image illustrating hTopo II based decatenation assay using kDNA. Lane 1 signifies kDNA with hTopo II, Lane 2 kDNA without hTopo II, Lane 3 etopoisde (E) used as positive control, Lane 4–8 investigational samples at 100 µM concentration; (B) Quantification of product formed in kDNA based decatenation assay. Blue represent positive control etoposide (E), red represent inactive compound (**4A**-**4C**) and green represents active compounds (**4D** and **4E**) w.r.t to etoposide.

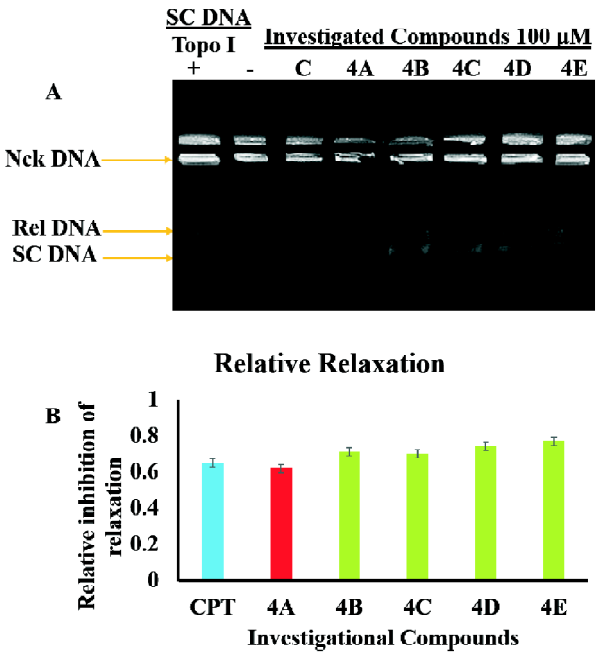

Fig. 4. (A) Agarose gel image illustrating results obtained for hTopo I relaxation assay. Lane 1 signifies plasmid DNA with hTopo I, Lane 2 plasmid DNA without hTopo I, Lane 3 camptothecin (C or CPT) used as positive control, Lane 4–8 investigational samples at 100 µM concentration; (B) Quantification of product formed in hTopo I relaxation assay. Blue represents positive control camptothecin (C or CPT), red represents inactive compound (**4A**) and green represents active compounds (**4B**-**4E**) w.r.t to CPT.

The work was further corroborated using molecular docking studies of **4E**. (**4E***R* and **4E***S* isomers) at the active site of hTopo I (PDB ID: 1T8I) and hTopo II (PDB entry: 3QX3). The bound CPT in hTopo I was used for comparing the interactions of **4E** in Topo I. The compound **4E***S* was found to have a better affinity as compared to **4E***R*. The cyano group of **4E***S* was found to interact and form H-bond with Thr718, whereas -NH_2 at the imidazole ring interacted with Arg364. The nitrogen of *N*-methylaniline and secondary -OH group also exhibited H-bond interaction with DT and TGP, respectively. The additional H-bond interactions could help increasing the binding affinity of the compounds to the hTopo I protein. The free aryl ring was found to occupy the active site surrounded by Asn352, Ala351, and Met428. Other notable interactions involved were π-π stacking of imidazole and phenyl ring with TGP (see Fig. 5A). Next, **4E***S* also occupied ATPase domain of hTopo II (PDB entry: 3QX3). The validation was performed by re-docking the etoposide into the

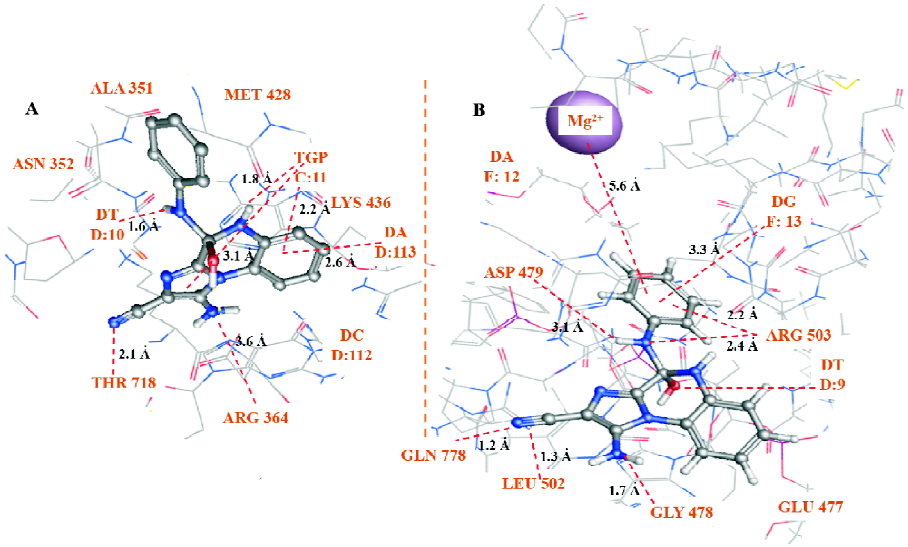

Fig. 5. 3D poses of **4E** illustrating its binding in active domain of (**A**) hTopo I (PDB ID: 1T8I) and, (**B**) hTopo II (PDB ID: 3QX3).

ATPase domain of hTopo II sugesting similar conformation to that of the co-crystal ligand with RMSD of 0.019. The important interaction that were observed (not shown) with etoposide includes the G478, D479, and L502 residues. H-bonding and weak van der Waals interactions were observed at Gln778 and Met782 glycosidic group of etoposides. The aglycone part of etoposide was found to be flanked between sugar bases of DNA. Further, the Gln778 residue (of β isoform) is reported to be replaced with Met762 in α-isoform that assist in the development of isoform-specific inhibitors of hTopo II[13]. All the important interactions displayed by etoposide were found to be conserved in TAS-103 and **4E***S*. The -CN group of **4E***S* was found to interact with Gln778 and Leu502. The Gly478 was found to interact with lone pair of the NH_2 group of imidazole. The phenolic and aryl ring were involved in π-π stacking with DG, with phenyl ring showing additional π-π stacking with Arg503. Lone pair of -NH (ring system) showed H-bond interaction with Arg503, whereas the secondary -OH group was involved in H-bonding with DT (see Fig. 5B).

Next, we were interested to know whether the hTopos inhibition via the target compound could lead to anticancer activity or not. To explore this, we tested the antiproliferative potential of all the compounds using MTT assay on three different cancer cell lines A-549 (lung cancer), HT-29 (colon cancer), and MDA-MB-231 (breast cancer). After 48 h of incubation with cancer cells at three varying concentrations of 1, 5, and 25 μM all the compounds were able to exhibit antiproliferative potential (IC_{50}) in the range of 1.8–8.3 μM (Table 1) and were comparable to positive control employed. Further, the selected molecules **4D** and **4E**, when tested on normal breast cells (HBL-100) at the highest concentration of 10 μM for 48 h (results not shown) exhibited no toxicity, thus proving their selective anticancer potential.

Table 1. Antiproliferative activity of synthetics **4A-4E**

Cd	Inhibitory potential (IC_{50} (μM) ± SD)[a]		
	A-549 (Lung cancer)	HT29 (Colon cancer)	MDA-MB-231 (Breast cancer)
4A	3.1±0.21	4.9±0.19	4.2±0.17
4B	3.8±0.31	7.2±0.27	3.5±0.13
4C	1.98±0.19	4.9±0.16	8.3±0.18
4D	7.2±0.2	2.7±0.13	3.8±0.21
4E	4.3±0.16	3.5±0.43	1.8±0.23
CPT	3.32±0.14	3.2±0.21	2.32±0.32

[a]Assay was performed in triplicate and at three different concentration.

To further investigate the secondary anticancer mechanism associated with the target compounds, the MDAMB-231 cells were treated with **4D** and **4E** at sub-IC_{50} concentration and incubated for 48 h. The results indicated that **4D** and **4E** were able to increase the ROS levels inside the cancer cells (MDA-MB-231) as analyzed by H_2DCFDA assay (Fig. 6A). The increased ROS often alters the mitochondrial

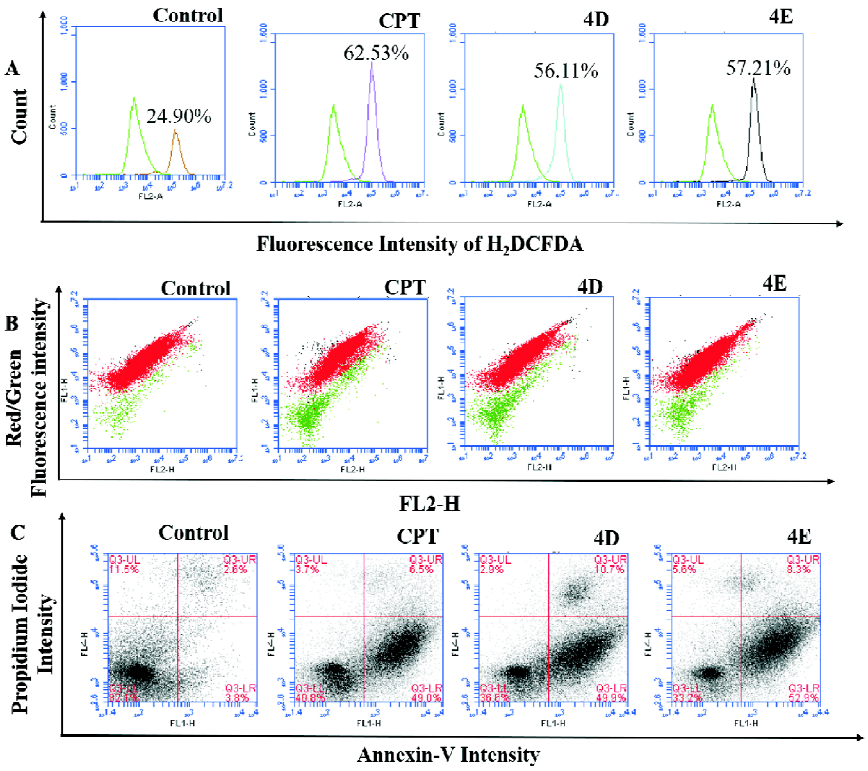

Fig. 6. (A) Illustrates relative fluorescence altered via influence of ROS generation upon treatment with investigational compounds in MDA-MB-231 cells as conferred by H_2DCFDA based assay; (B) Quantification ratio plots depicting J-aggregates/J-monomers depicting mitochondrial membrane permeability as detected by JC-1 dye; (C) Propidium Iodide vs Annexin-V depicting mode of cell death upon treatment investigational compounds in MDA-MB-231 cells.

permeability and to understand the effect, JC-1 assay was performed. The assay revealed (Fig. 6B) **4D**, and **4E** were able to alter mitochondrial permeability (decrease in red/green ratio), leading to apoptosis as analyzed via PI vs Annexin-V assay (Fig. 6C).

Conclusions

In conclusion, we designed **4A-4E** as the dual inhibitors of hTopos using molecular modeling techniques. The synthesis of target compounds **4A-4E** was achieved viaring closure reactions of **4** with electrophiles through Pictet-Spengler (PS) reaction. The biological evaluation of the synthetics was performed to assess the anticancer potential via dual inhibition of Topo I and II. The compounds **4D** and **4E** emerged as dual inhibitors of hTopo I and II with selective anticancer potential. The compounds also induced an increase in ROS, alteration in mitochondrial permeability leading to cell death via apoptosis. The molecular docking highlighted the binding interactions of the compounds with both the enzymes. The future research work would include their assessment in *in vivo* cancer models.

Acknowledgments

The authors are thankful to Vice-Chancellor and Dean In-charge, Central University of Punjab, Bathinda, for providing the funds to support the present work. The authors also acknowledge CIL and funding provided by DST-FIST to the department. RK also thanks DST-SERB, New Delhi (Grant no. EMR/2017/002702/HS), for the extramural research grant. GJ thanks Dr. Sandeep Singh (Associate Professor, Department of Human Genetics and Molecular Medicine, School of Health Sciences, Central University of Punjab, Bathinda) for assisting in biological studies.

References

1. (a) A. J. Bannister and T. Kouzarides, *Cell Research,* 2011, **21**, 381; (b) C. Bailly, *Chem. Rev.,* 2012, **112**, 3611; (c) Y. Pommier, *Nat. Rev. Cancer,* 2006, **6**, 789; (d) Y. Pommier, E. Leo, H. Zhang and C. Marchand, *Chem. Biol.,* 2010, **17**, 421; (e) Y. Pommier,

Chem. Rev., 2009, **109**, 2894; (f) G. Joshi, "Synthesis and Biological Evaluation of Inhibitors of Topoisomerases and Histone Deacetylase For In Vitro Anticancer Activity", Central University of Punjab, India.

2. (a) H. Lincet and P. Icard, *Oncogene,* 2015, **34**, 3751; (b) E. Baldwin and N. Osheroff, *Curr. Med. Chem. Anticancer Agents,* 2005, **5**, 363; (c) B. Dwarakanath, D. Khaitan and R. Mathur, *Indian J. Exp. Biol.,* 2004, **42**, 649; (d) G. Joshi, S. M. Amrutkar, A. T. Baviskar, H. Kler, S. Singh, U. C. Banerjee and R. Kumar, *RSC Adv.,* 2016, **6**, 14880; (e) A. Negi, J. M. Alex, S. M. Amrutkar, A. T. Baviskar, G. Joshi, S. Singh, U. C. Banerjee and R. Kumar, *Bioorg. Med. Chem.,* 2015, **23**, 5654.
3. (a) R. Kumar, U. C. Banerjee, S. M. Amrutkar, A. T. Baviskar, S. Singh, G. Joshi and H. Kler, *RSC Adv.,* 2016, **6**, 14880; (b) J. R. Jenkins, P. Ayton, T. Jones, S. L. Davies, D. L. Simmons, A. L. Harris, D. Sheer and I. D. Hickson, *Nucleic Acids Res.,* 1992, **20**, 5587; (c) R. N. Ganapathi and M. K. Ganapathi, *Front Pharmacol.,* 2013, **4**, 89.
4. S. Salerno, F. Da Settimo, S. Taliani, F. Simorini, C. La Motta, G. Fornaciari and A. M Marini, *Curr. Med. Chem.,* 2010, **17**, 4270.
5. (a) D. Chakraborty, C. K. Jain, A. Maity, S. Ghosh, S. R. Choudhury, T. Jha, H. K. Majumder and N. B. Mondal, *MedChemComm.,* 2016, **7**, 837; (b) J. Janoèková, J. Plšíková, J. Kašpárková, V. Brabec, R. Jendželovský, J. Mikeš, J. Koval', S. Hamul'aková, P. Fedoročko and K. Kuča, *Eur. J. Pharm. Sci.,* 2015, **76**, 192; (c) B.-L. Yao, Y.-W. Mai, S.-B. Chen, H.-T. Xie, P.-F. Yao, T.-M. Ou, J.-H. Tan, H.-G. Wang, D. Li and S.-L. Huang, *Eur. J. Med. Chem.,* 2015, **92**, 540; (d) J. Janockova, J. Plšíková, R. Jendzelovsky, J. Mikes, J. Kasparkova, V. Brabec, S. Hamulakova, P. Fedoroako and M. Kozurkov, *Bioorg. Chem.,* 2015, **59**, 168; (e) R. Karki, K.-Y. Jun, T. M. Kadayat, S. Shin, T. B. T. Magar, G. Bist, A. Shrestha, Y. Na, Y. Kwon and E.-S. Lee, *Eur. J. Med. Chem.,* 2016, **113**, 228.
6. (a) N. Vicker, L. Burgess, I. S. Chuckowree, R. Dodd, A. J. Folkes, D. J. Hardick, T. C. Hancox, W. Miller, J. Milton and S. Sohal, *J. Med. Chem.,* 2002, **45**, 721; (b) B. Poddevin, J.-F. Riou, F. Lavelle and Y. Pommier, *Mol. Pharmacol.,* 1993, **44**, 767; (c) B. Montaner, W. Castillo-Avila, M. Martinell, R. Öllinger, J. Aymami, E. Giralt and R. Pérez-Tomás, *Toxicological Sciences,* 2005, **85**, 870; (d) G. Joshi, S. Kalra, U. P. Yadav, P. Sharma, P. K. Singh, S. Amrutkar, A. J. Ansari, S. Kumar, A. Sharon and S. Sharma, *Bioorg. Chem.,* 2020, **94**, 103409.
7. (a) A. M. Azarova, Y. L. Lyu, C.-P. Lin, Y.-C. Tsai, J. Y.-N. Lau, J. C. Wang and L. F. Liu, *Proc. Natl. Acad. Sci.,* 2007, **104**, 11014; (b) A. R. Mistry, C. A. Felix, R. J. Whitmarsh, A. Mason, A. Reiter, B. Cassinat, A. Parry, C. Walz, J. L. Wiemels and M. R. Segal, *N. Engl. J. Med.,* 2005, **352**, 1529; (c) C. A. Felix, *Biochim. Biophys. Acta, Gene Struct. Expression,* 1998, **1400**, 233.
8. (a) J. P. Eder, V. Chan, J. Wong, Y. W. Wong, G. Ara, D. Northey, N. Rizvi and B. A. Teicher, *Cancer Chemother. Pharmacol.,* 1998, **42**, 327; (b) J. A. Houghton, P. J. Cheshire, J. D. Hallman, L. Lutz, X. Luo, Y. Li and P. J. Houghton, *Clin. Canc. Res.,* 1996, **2**, 107; (c) M. Crump, J. Lipton, D. Hedley, D. Sutton, F. Shepherd, M. Minden, K. Stewart, S. Beare and E. Eisenhauer, *Leukemia,* 1999, **13**, 343; (d) T. Simon, A. Langler, F. Berthold, T. Klingebiel and B. Hero, *J. Pediatr. Hematol. Oncol.,* 2007, **29**, 101; (e) H. J. Choi, B. C. Cho, S. J. Shin, S. H. Cheon, J. Y. Jung, J. Chang, S. K. Kim, J. H. Sohn and J. H. Kim, *Cancer Chemother. Pharmacol.,* 2008, **61**, 309.
9. (a) R. Kumar, R. K. Ujjinamatada and R. S. Hosmane, *Org. Lett.,* 2008, **10**, 4681; (b) S. Kalra, G. Joshi, M. Kumar, S. Arora, H. Kaur, S. Singh, A. Munshi and R. Kumar, *RSC Medicinal Chemistry,* 2020. doi.org/10.1039/D0MD00146E.
10. G. Joshi, M. Chauhan, R. Kumar, A. Thakur, S. Sharma, R. Singh, A. A. Wani, A. Sharon, P. V. Bharatam and R. Kumar, *Org. Chem. Front.,* 2018, **5**, 3526.
11. (a) J. F. Carey, S. J. Schultz, L. Sisson, T. G. Fazzio and J. J. Champoux, *Proc. Natl. Acad. Sci.,* 2003, **100**, 5640; (b) T. J. Wendorff, B. H. Schmidt, P. Heslop, C. A. Austin and J. M. Berger, *J. Mol. Biol.,* 2012, **424**, 109.
12. B. L. Staker, M. D. Feese, M. Cushman, Y. Pommier, D. Zembower, L. Stewart and A. B. Burgin, *J. Med. Chem.,* 2005, **48**, 2336.
13. C.-C. Wu, T.-K. Li, L. Farh, L.-Y. Lin, T.-S. Lin, Y.-J. Yu, T.-J. Yen, C.-W. Chiang and N.-L. Chan, *Science,* 2011, **333**, 459.
14. (a) A. J. Ansari, G. Joshi, U. P. Yadav, A. K. Maurya, V. K. Agnihotri, S. Kalra, R. Kumar, S. Singh and D. M. Sawant, *Bioorg. Chem.,* 2019, **93**, 103314; (b) G. Joshi, H. Nayyar, S. Kalra, P. Sharma, A. Munshi, S. Singh and R. Kumar, *Chem. Biol. Drug. Des.,* 2017, **90**, 995; (c) D. M. Sawant, S. Sharma, R. S. Pathare, G. Joshi, S. Kalra, S. Sukanya, A. K. Maurya, R. K. Metre, V. K. Agnihotri and S. Khan, *Chem. Comm.,* 2018, **54**, 11530.